gained from observing the breakup of dimer ions, for example:

$$(CH_4)_2+e\rightarrow(CH_4\cdots CH_4)^++2e\rightarrow\text{product ions}$$

may have a bearing on models and predictions of ion–molecule reactions insofar as the $(CH_4–CH_4)^+$ parent cluster-ion approximates the transition state in the $CH_4+CH_4^+$ ion–molecule reaction.[22]

ACKNOWLEDGMENT

This work was supported by the Power Branch of the Office of Naval Research under Contract No. Nonr-3599(00).

[1] T. A. Milne and F. T. Greene, Advan. Chem. Ser. **72,** 68 (1968).
[2] F. T. Greene, J. Brewer, and T. A. Milne, J. Chem. Phys. **40,** 1488 (1964).
[3] H. Ashkenas and F. S. Sherman, *Fourth Rarefied Gas Dynamics Symposium*, (Academic, New York, 1965), Vol. 2, p. 84.
[4] O. Osberghaus and R. Taubert, Z. Phys. Chem. **4,** 264 (1955).
[5] T. A. Milne and F. T. Greene, *Advances in High Temperature Chemistry*, edited by L. Eyring, (Academic, New York, 1969), Vol. II, p. 107.
[6] J. B. Anderson, R. P. Andres, and J. B. Fenn, *Advances in Chemical Physics*, edited by John Ross (Interscience, New York, 1966), Vol. X, p. 275.
[7] L. Trilling and H. Y. Wachman (Eds.), *Sixth Rarefied Gas Dynamics Symposium*, Vols. 1 and 2 (Academic, New York 1969), Vol. 1 and 2. (See also earlier Symposia.)
[8] D. R. Miller and R. P. Andres, J. Chem. Phys. **46,** 3418 (1967).
[9] O. Hagena and W. Henkes, Z. Naturforsch. **A15,** 851 (1960).
[10] A. K. Robrov and R. G. Sharafutdinov, *Sixth Rarefied Gas Dynamics Symposium* (Academic Press, New York, 1969), Vol. 2, p. 965.
[11] J. W. Rich and C. E. Treanor, Ann. Rev. Fluid Mech. **2,** 355 (1970).
[12] V. K. Konyukhov, I. V. Matrosov, A. M. Prokhorov, P. T. Shalunov, and N. N. Shirokov, ZhETF Pis. Red. **10,** 84 (1969).
[13] W. A. Chupka, "Proceedings of the High Pressure Sampling Conference," Midwest Research Institute, 1965.
[14] H. M. Rosenstock, Advan. Mass Spectry. **4,** 523 (1968).
[15] A. Cassuto, Advan. Mass Spectry. **2,** 296 (1961).
[16] T. A. Milne, and F. T. Greene, J. Chem. Phys. **47,** 4095 (1967).
[17] T. A. Milne, J. E. Beachey, and F. T. Greene, "Detection of Argon Cluster Fragmentation in a Time-of-Flight Mass Spectrometer," J. Chem. Phys. (to be published).
[18] S. N. Foner and R. L. Hundson, J. Chem. Phys. **21,** 1374 (1953).
[19] S. N. Foner and R. L. Hudson, J. Chem. Phys. **36,** 2676 (1962).
[20] S. N. Foner and R. L. Hudson, J. Chem. Phys. **36,** 3681 (1962).
[21] T. A. Milne and F. T. Greene, J. Chem. Phys. **44,** 2444 (1966).
[22] A. Henglein, in *Molecular Beams and Reaction Kinetics*, edited by Charles Schlier (Academic, New York, 1970), p. 146.

THE JOURNAL OF CHEMICAL PHYSICS VOLUME 56, NUMBER 6 15 MARCH 1972

Studies in Molecular Dynamics. X. Corrections to the Augmented van der Waals Theory for the Square Well Fluid*

B. J. Alder, D. A. Young, and M. A. Mark†
Lawrence Livermore Laboratory, University of California, Livermore, California 94550

(Received 14 October 1971)

The validity of the augmented van der Waals theory of fluids is demonstrated by a rigorous evaluation of the next three terms in the reciprocal temperature expansion of the Helmholtz free energy for the square-well fluid. Each term in the dense fluid is shown to be an order of magnitude smaller than the preceding one except the fourth, which is comparable to the third. Analysis of molecular dynamics data leads to a peak in the heat capacity at the coexistence curve which is not reproduced by the finite series. This peak in turn leads to realistic values of the critical indices α and α', while the other indices β, γ, and δ have their classical van der Waals values.

I. INTRODUCTION

In a recent paper the augmented van der Waals theory was discussed.[1] This theory was obtained by considering a perturbation expansion to first order of the free energy of a fluid of hard spheres with added attractive potentials which must be weak relative to the kinetic energy. This calculation yields an equation of state equivalent to the classical van der Waals result,[2] except that exact, rather than approximate hard sphere properties are introduced. Thus, in the rigorous theory, what used to be the classical van der Waals constant "a" becomes a density-dependent function. This so-called "augmented van der Waals theory" predicts the thermodynamic properties of a number of model fluids with remarkable accuracy even at temperatures where the attractive potential energy is no longer small compared to the kinetic energy.

The purpose of this paper is to understand why the first order theory converges so well, or alternatively, why the higher order terms are so small. Hence this paper is devoted to an accurate calculation of the terms beyond first order in the perturbation expansions of the free energy and pressure by several alternative methods. The perturbation expansion prediction of thermodynamic properties is then compared with results obtained directly from molecular dynamics computations in order to evaluate the convergence of the expansion. Special attention is given to the critical region as a severe test of the theory.

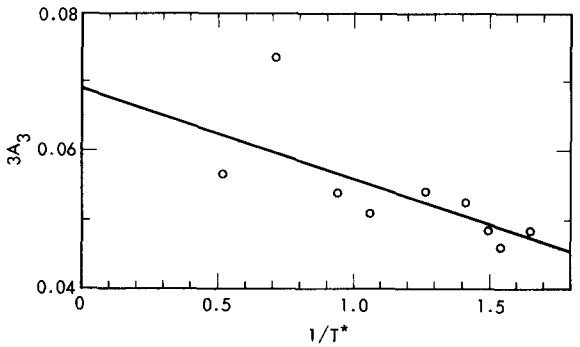

FIG. 1. Example of a calculation of A_3 from molecular dynamics excess internal energy data for $V/V_0=1.6$. The circles are values of $[E^E-E_0-E_1/T^*]T^{*2}$ plotted against $1/T^*$. The intercept of the straight line through the data points leads to $A_3=0.023$.

II. PERTURBATION THEORY

For a system of hard spheres with added attractive pair potentials a Taylor expansion of the reduced excess Helmholtz free energy about the infinite temperature limit can be written as

$$\frac{A^E}{NkT}=\frac{A-A^I}{NkT}=\frac{A_0{}^E}{NkT}+\left[\frac{\partial(A^E/NkT)}{\partial\beta}\right]_0\beta+\frac{1}{2}\left[\frac{\partial^2(A^E/NkT)}{\partial\beta^2}\right]_0\beta^2+\frac{1}{6}\left[\frac{\partial^3(A^E/NkT)}{\partial\beta^3}\right]_0\beta^3+\cdots, \tag{1}$$

where A^E, A, A^I, and $A_0{}^E$ are the excess, total, ideal gas, and excess hard sphere Helmholtz free energies, respectively, and $\beta=1/kT$. The above derivatives can be re-expressed by means of well known thermodyanmic relations:

$$\left[\frac{\partial(A^E/NkT)}{\partial\beta}\right]_0=\lim_{T\to\infty}\frac{E^E}{N};$$

$$\left[\frac{\partial^2(A^E/NkT)}{\partial\beta^2}\right]_0=\lim_{T\to\infty}-\frac{kT^2C_V{}^E}{N};$$

and

$$\left[\frac{\partial^3(A^E/NkT)}{\partial\beta^3}\right]_0=\lim_{T\to\infty}\left(2k^2T^3C_V{}^E+k^2T^4\frac{dC_V{}^E}{dT}\right)\Big/N,$$

where E^E and $C_V{}^E$ are the excess internal energy and heat capacity, respectively. Since the coefficients are evaluated in the infinite temperature limit ($\beta=0$) in the above expansions, they can be identified as thermodynamic averages evaluated in the hard sphere fluid.

A statistical mechanical expansion equivalent to Eq. (1) can be derived[3]:

$$A^E-A_0{}^E=\sum_{n=1}^{\infty}\frac{\omega_n}{n!}(-\beta)^{n-1}, \tag{2}$$

where $A_0{}^E$ is, as before, the excess hard sphere Helmholtz free energy. The ω_n's contain moments of the perturbing potential averaged over hard sphere distribution functions. Calculation of ω_n requires distribution functions of all orders up to $2n$. The general expression[3] for ω_j is given by

$$\omega_j=j!\sum_{n_s,(\Sigma sn_s=j)}(-1)^{\Sigma n_s-1}(\Sigma n_s-1)!\prod_{s=1}^{\infty}(n_s!)^{-1}\times\left(\frac{\langle V^s\rangle_0}{s!}\right)^{n_s}. \tag{3}$$

The quantity $\langle V^s\rangle_0$ is the s power of the perturbing potential V evaluated in the hard sphere limit. From Eq. (3) $\omega_1=\langle V\rangle_0$, which means that the coefficient of β in the expansion of A^E/NkT [Eq. (1)] is $\langle V\rangle_0/N$. But this is precisely the coefficient given in the thermodynamic identification of Eq. (1), since $\langle V\rangle=E^E$. Similarly $\omega_2=\langle V^2\rangle_0-\langle V\rangle_0{}^2$, so the coefficient of β^2 in Eq. (1) is $-(\langle V^2\rangle_0-\langle V\rangle_0{}^2)/2N$. This is again identical to the expression involving $C_V{}^E$ in the thermodynamic expansion, as can be shown by twice differentiating the canonical ensemble partition function with respect to β. Corresponding coefficients in Eqs. (1) and (2) are all identical, and the two expansions provide separate but equivalent methods for the calculation of the coefficients in the free energy expansion.

Molecular dynamics calculations may be employed in both of the ways suggested above. Thermodynamic quantities may be computed directly as functions of temperature for the model potential and then extrapolated to $T=\infty$. This is done for the excess internal energy and the pressure. Alternatively, statistical averages of the attractive part of the pair potential may be computed directly by molecular dynamics in a fluid of hard spheres. The attractive potential used is a

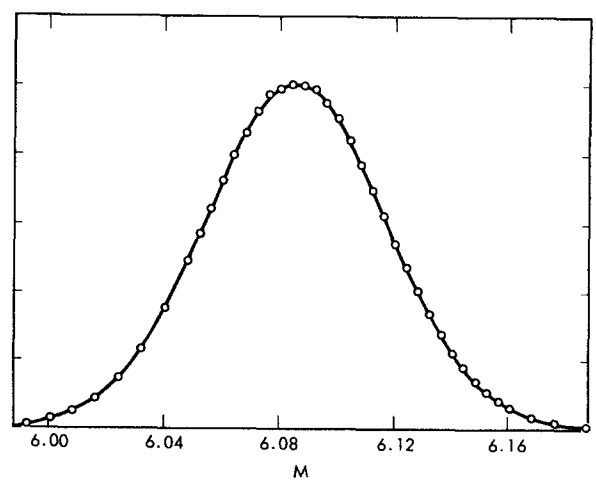

FIG. 2. The frequency of occurrence of square-well pair interactions plotted against the number of interactions per particle, M, for a system of 500 particles at $V/V_0=1.6$. The points are obtained from molecular dynamics, and the smooth curve is a Gaussian obtained by a best fit through the points.

TABLE I. Ratios of moments of the distribution of pair interactions for hard sphere fluids with imaginary square wells. These ratios would all be unity if the distribution were Gaussian.

V/V_0	N	$\frac{\langle(M-\langle M\rangle)^4\rangle}{3\langle(M-\langle M\rangle)^2\rangle^2}$	$\frac{\langle(M-\langle M\rangle)^6\rangle}{15\langle(M-\langle M\rangle)^2\rangle^3}$	$\frac{\langle(M-\langle M\rangle)^8\rangle}{105\langle(M-\langle M\rangle)^2\rangle^4}$
1.5	108	1.02	1.05	1.09
1.5	500	1.01	1.02	1.05
1.6	108	1.00	0.99	0.98
1.6	500	1.02	1.08	1.23
2.0	108	1.01	1.04	1.08
2.0	500	1.00	1.02	1.06
3.0	108	1.01	1.02	1.03
3.0	500	0.99	0.98	0.98
7.071	108	1.00	1.02	1.04

square well of width one half the hard sphere diameter and depth ϵ.

Eq. (1) may be rewritten as

$$\frac{A^E}{NkT}=\frac{A_0{}^E}{NkT}+\sum_{n=1}^{\infty}\frac{A_n}{T^{*n}}, \tag{4}$$

where $T^*=kT/\epsilon$ and $A_n=-\omega_n/[n!(-\epsilon)^nN]$. The dimensionless coefficients A_n require the evaluation of sums of terms such as $\langle V^n\rangle/(-\epsilon)^n$. In the square-well molecular dynamics program these terms are especially simple to calculate because $\langle V^n\rangle/(-\epsilon)^n=\langle M^n\rangle$, where M is the number of pairs of interacting particles.[4] Since M is always an integer in any given configuration, the distribution of M about its average value can be obtained exactly, and the moments of the distribution required by the A_n's may then be computed as a finite sum. Working with powers of the sum M avoids the virtually impossible task of directly evaluating higher order distribution functions and taking averages over them.

TABLE II. Values of A_1 obtained from both the extrapolation of square-well internal energy data (E) and from hard sphere fluctuation averages (HS).

		$-A_1$	
V/V_0	N	HS	E
1.5	500	6.387	
1.6	108	6.101	6.135
1.6	500	6.085	
1.7	108		5.796
1.8	108	5.480	5.468
2.0	108	4.923	4.923
2.0	500	4.924	
2.2	108	4.435	
2.4	108	4.018	
2.5	108		3.83
2.6	108	3.662	
3.0	108	3.093	3.084
3.0	500	3.099	
4.0	108		2.170
5.0	108		1.617
7.071	108	1.138	

In summary, the A_n's up to A_4 are given in both thermodynamic and statistical mechanical form. In the evaluation of Eq. (3) for ω_n, the moment terms have been grouped into fluctuations of M about its average value:

$$A_1=-\langle M\rangle/N=\lim_{T^*\to\infty}(E^E/N\epsilon),$$

$$A_2=-\langle(M-\langle M\rangle)^2\rangle/2N=-\tfrac{1}{2}\lim_{T^*\to\infty}(T^{*2}C_V{}^E/Nk),$$

$$A_3=-\frac{\langle(M-\langle M\rangle)^3\rangle}{6N}=\tfrac{1}{6}\lim_{T^*\to\infty}\left(\frac{2T^{*3}C_V{}^E}{Nk}+\frac{T^{*4}}{Nk}\frac{dC_V{}^E}{dT^*}\right),$$

$$A_4=-[\langle(M-\langle M\rangle)^4\rangle-3\langle(M-\langle M\rangle)^2\rangle^2]/24N$$

$$=-\tfrac{1}{24}\lim_{T^*\to\infty}\left(\frac{6T^{*4}C_V{}^E}{Nk}+\frac{6T^{*5}}{Nk}\frac{dC_V{}^E}{dT^*}+\frac{T^{*6}}{Nk}\frac{d^2C_V{}^E}{dT^{*2}}\right). \tag{5}$$

Any thermodynamic quantity for the square-well fluid may be expressed in terms of the A_n's. In particular, the excess internal energy, excess heat capacity, and pressure are given below:

$$\frac{\partial(A^E/NkT)}{\partial(1/T^*)}=\frac{E^E}{N\epsilon}=\sum_{n=1}^{\infty}nA_n\left(\frac{1}{T^*}\right)^{n-1}, \tag{6}$$

$$-\frac{1}{T^{*2}}\frac{\partial^2(A^E/NkT)}{\partial(1/T^*)^2}=\frac{C_V{}^E}{Nk}=-\sum_{n=2}^{\infty}n(n-1)A_n\left(\frac{1}{T^*}\right)^n, \tag{7}$$

$$-\frac{\partial(A/NkT)}{\partial(V/V_0)}=\frac{pV_0}{NkT}=\frac{p_0V_0}{NkT}+\sum_{n=1}^{\infty}\left[-\frac{\partial A_n}{\partial(V/V_0)}\right]\left(\frac{1}{T^*}\right)^n=\frac{p_0V_0}{NkT}+\sum_{n=1}^{\infty}\frac{p_n}{T^{*n}}. \tag{8}$$

TABLE III. Values of A_2 obtained from both the extrapolation of square-well internal energy data (E) and from hard sphere fluctuation averages (HS)

		$-A_2$	
V/V_0	N	HS	E
1.5	500	0.215±0.001	
1.6	108	0.256±0.003	0.252±0.005
1.6	500	0.249±0.004	
1.7	108		0.27±0.01
1.8	108	0.296±0.006	0.30±0.02
2.0	108	0.306±0.006	0.30±0.01
2.0	500	0.301±0.005	
2.2	108	0.313±0.005	
2.4	108	0.306±0.004	
2.6	108		0.296±0.006
3.0	108	0.306±0.002	0.32±0.01
3.0	500	0.311±0.002	
4.0	108		0.32±0.02
4.5	108		0.32±0.02
5.0	108		0.30±0.02
5.766	108		0.31±0.05
6.0	108		0.31±0.02
7.0	108		0.27±0.04
7.071	108	0.288±0.002	

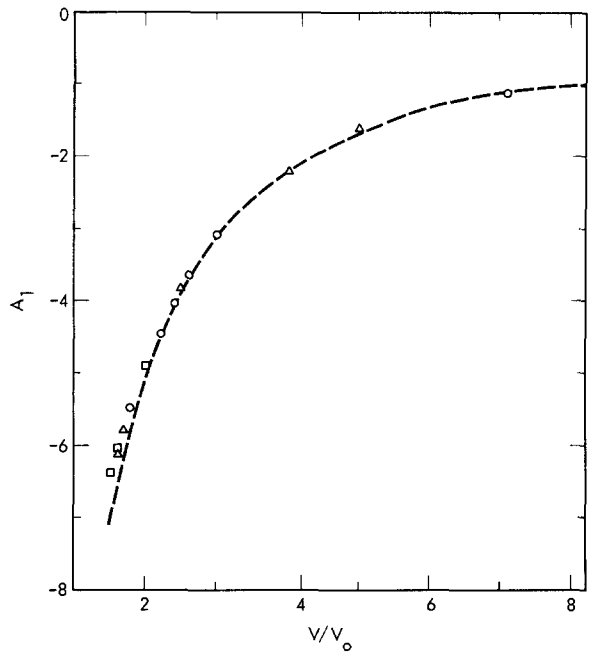

FIG. 3. A plot of A_1 against V/V_0. The circles (108 particles) and squares (500 particles) are obtained from molecular dynamics hard sphere data, and the triangles are obtained from extrapolation of square-well data. The dashed curve represents the contribution to A_1 from the first four virial coefficients of the square-well potential.

In Eq. (8) p is the total, rather than the excess, pressure.

III. METHOD OF CALCULATION

A large number of molecular dynamics calculations have been made on the square-well fluid at various relative volumes V/V_0, where V_0 is the close packed volume, and temperatures T^*. The range covered is $1.5 \leq V/V_0 < 7.1$ and $0.2 < T^* \leq \infty$. In each run the excess internal energy and the pressure have been calculated, and for certain cases the excess heat capacity has also been calculated. These data are tabulated in Appendix I.

TABLE IV. Values of A_3 obtained from the extrapolation of square-well internal energy data (E), from hard sphere fluctuation averages (HS), and from temperature dependent values of A_2 (A).

		A_3		
V/V_0	N	HS	E	A
1.5	500	0.033±0.04		
1.6	108	0.011±0.006	0.023±0.005	0.018±0.003
1.6	500	0.013±0.026		
2.0	108	0.00±0.01		−0.005±0.005
2.5	108		−0.018±0.005	
3.0	108	−0.025±0.009	−0.029±0.006	−0.025±0.008
3.0	500	−0.019±0.026		
3.5	108		−0.035±0.009	
4.0	108		−0.054±0.014	
4.5	108		−0.053±0.010	
5.0	108		−0.049±0.014	
5.766	108		−0.065±0.011	
6.0	108		−0.060±0.014	
7.0	108		−0.054±0.014	
7.071	108	−0.065±0.006		

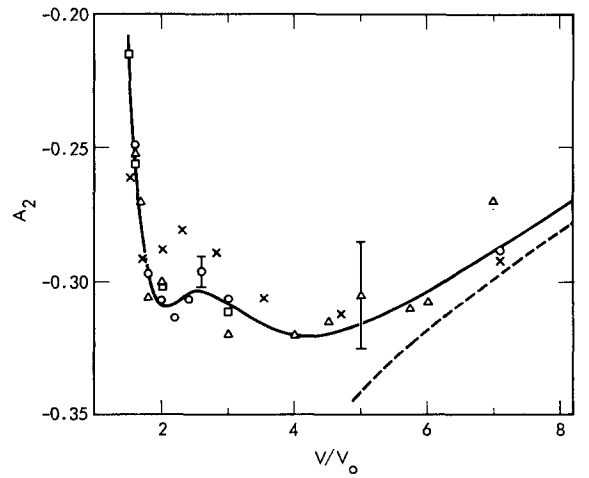

FIG. 4. A plot of A_2 against V/V_0. The circles (108 particles) and squares (500 particles) are obtained from molecular dynamics hard sphere data, and the triangles are obtained from extrapolation of square-well data. The crosses are from the approximate calculation of Barker and Henderson (Ref. 4). The solid curve is the best fit through the data points. The dashed curve is the contribution to A_2 from the first four virial coefficients of the square-well potential. Typical error bars are shown.

TABLE V. Values of A_4 obtained from the extrapolation of square-well internal energy data (E), from hard sphere fluctuation averages (HS), and from temperature dependent values of A_2 ($A2$) and A_3 ($A3$).

		A_4			
V/V_0	N	HS	E	$A2$	$A3$
1.6	108	0.023±0.015	−0.002±0.002	−0.002±0.002	0.006±0.001
2.0	108		0.004±0.004	0.003±0.003	0.007±0.001
3.0	108	−0.042±0.035	−0.019±0.003	−0.019±0.003	−0.016±0.004
3.5	108		−0.017±0.007		
4.0	108		−0.019±0.004		
4.5	108		−0.030±0.005		
5.0	108		−0.032±0.007		
5.766	108		−0.035±0.010		
6.0	108		−0.028±0.007		
7.0	108		−0.032±0.010		
7.071	108	−0.031±0.015			

Each thermodynamic function may be written as a power series in $1/T^*$. In the case of the excess internal energy,

$$\frac{E^E}{N\epsilon} = \sum_{n=0}^{\infty} E_n \left(\frac{1}{T^*}\right)^n. \tag{9}$$

The quantity E_0 is obtained by first plotting $E^E/N\epsilon$ as a function of $1/T^*$ for a given V/V_0 and then extrapolating this curve to $1/T^*=0$. The quantity E_1 is obtained by plotting $(E^E/N\epsilon - E_0)T^*$ vs $1/T^*$ and extrapolating to zero. This process of subtraction and extrapolation is continued until the errors in the data overwhelm the coefficients being calculated. With this method coefficients up to A_4 may be computed. An example of the calculation of A_3 at $V/V_0=1.6$ is given in Fig. 1. The A_n's may be obtained from the E_n's by the relation [see Eq. (6)] $A_n=E_{n-1}/n$. A similar procedure is followed with the pressure in order to calculate the coefficients p_n. With this method coefficients up to p_3 may be obtained.

The molecular dynamics calculations have been

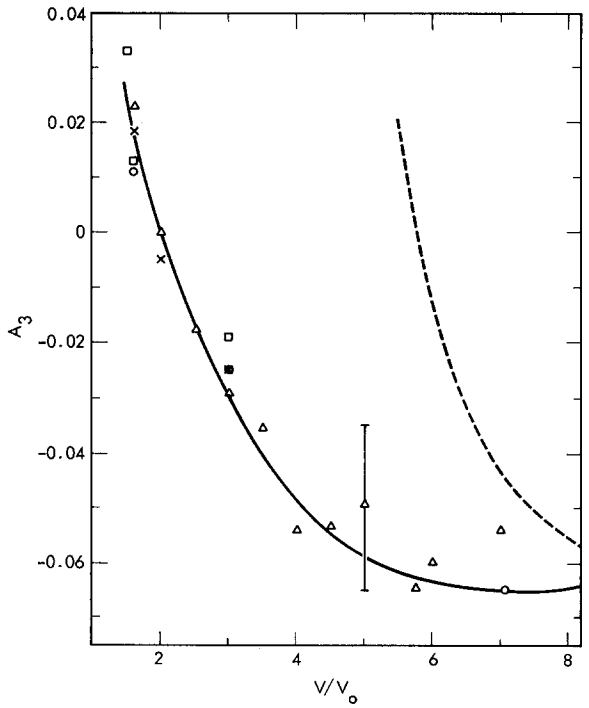

FIG. 5. A plot of A_3 against V/V_0. The circles (108 particles) and squares (500 particles) are obtained from molecular dynamics hard sphere data, the triangles are obtained from the extrapolation of square-well data, and the crosses obtained from the extrapolation of A_2 data. The solid curve is the best fit through the data points. The dashed curve is the contribution to A_3 from the first four virial coefficients of the square-well potential. A typical error bar is shown.

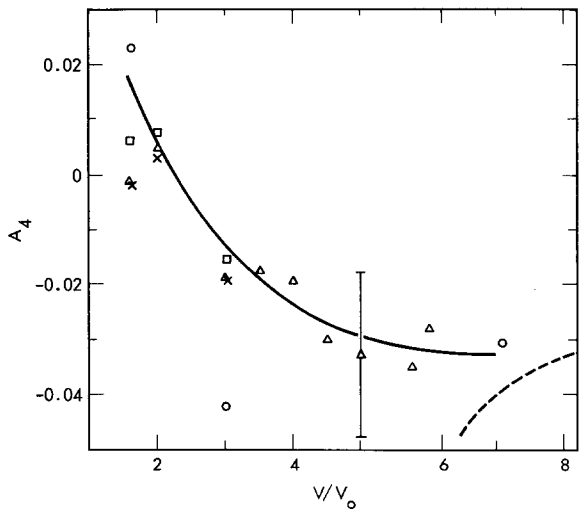

FIG. 6. A plot of A_4 against V/V_0. The circles are obtained from 108 particle molecular dynamics hard sphere data, the triangles from the extrapolation of square-well data, the crosses from the extrapolation of A_2 data, and the squares from the extrapolation of A_3 data. The solid curve is the best fit through the data points. The dashed curve is the contribution to A_4 from the first four virial coefficients of the square-well potential. A typical error bar is shown.

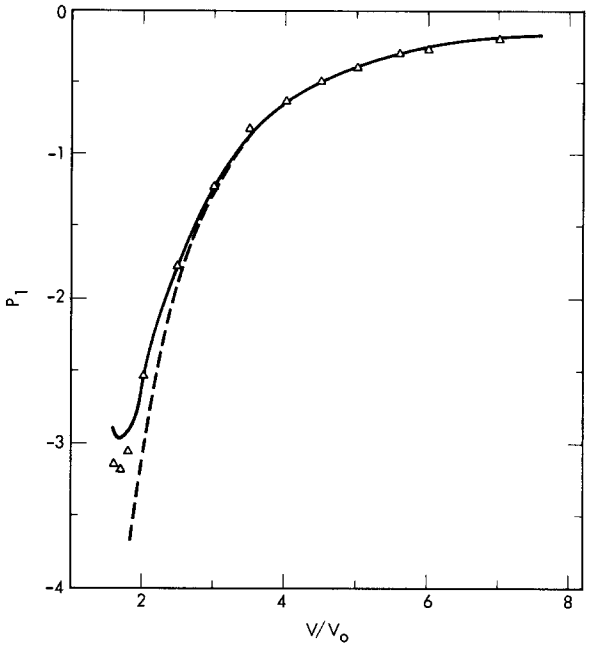

FIG. 7. A plot of p_1 against V/V_0. The triangles are obtained from extrapolation of square-well data. The smooth curve is the volume derivative of the best fit of the A_1 data (Fig. 3). The dashed curve is the contribution to p_1 from the first four virial coefficients of the square-well potential. The virial approximation becomes identical with the fit for $V/V_0>3.5$.

carried out for systems of 32, 108, and 500 particles. The excess energy E^E/N is number dependent, but this dependence shows up strongly only at low temperature. Hence it is difficult to determine the number dependence of the coefficients in the infinite temperature limit. Since the data are most numerous for $N=108$, the coefficients listed in tables are calculated from 108 particle data. The number dependence of the pressure is too small to be detected.

In the direct calculation of the statistical averages in Eq. (5), the molecular dynamics program is used to simulate a hard sphere fluid with imaginary square wells. The square wells are "imaginary" in the sense that they have no effect on the dynamics of the hard spheres. This is the meaning of the infinite temperature limit. At every hard sphere collision the number of virtual pair interactions M is computed and tabulated. An error is introduced by computing averages only at collisions and not over all phase space, but this error is too small to be detected within the accuracy of the calculation for the volume range we have chosen. The coefficients A_n in the expansion of the free energy are composed of average values of fluctuations about $\langle M\rangle$. As previously mentioned, the M distribution is exactly known because the M's are integers, and hence the fluctuation moments of the distribution can be calculated as a finite sum. These moments have been computed up to $\langle(M-\langle M\rangle)^8\rangle$.

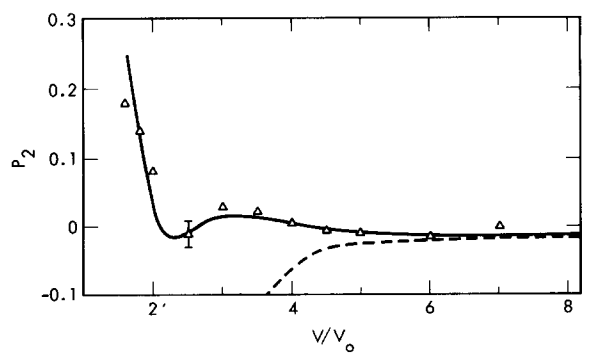

FIG. 8. A plot of p_2 against V/V_0. The triangles are obtained from the extrapolation of square-well data. The smooth curve is the volume derivative of the best fit to the A_2 data (Fig. 4). The dashed curve is the contribution to p_2 from the first four virial coefficients of the square-well potential. A typical error bar is shown.

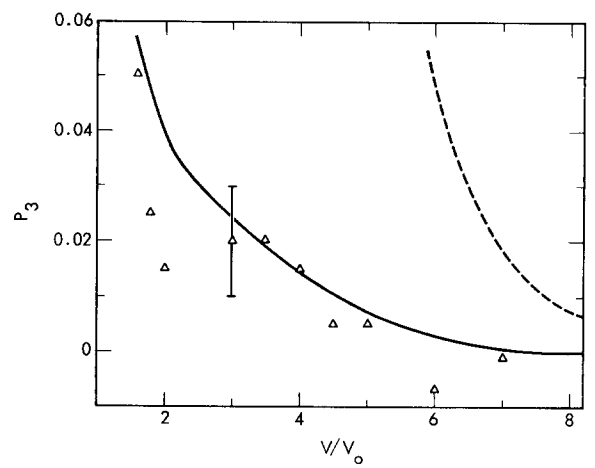

FIG. 9. A plot of p_3 against V/V_0. The triangles are obtained from the extrapolation of square-well data. The smooth curve is the volume derivative of the best fit to the A_3 data (Fig. 5). The dashed curve is the contribution to p_3 from the first four virial coefficients of the square-well potential. A typical error bar is shown.

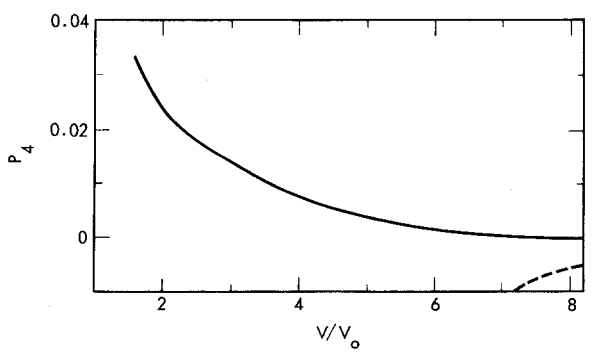

FIG. 10. A plot of p_4 against V/V_0. No square-well data are available. The smooth curve is the volume derivative of the best fit to the A_4 data (Fig. 6). The dashed curve is the contribution to p_4 from the first four virial coefficients of the square-well potential.

TABLE VI. Values of p_1, p_2, and p_3 obtained from the extrapolation of square-well equation of state data. A single typical uncertainty value is given for p_3.

V/V_0	p_1	p_2	p_3
1.6	−2.92±0.05	0.18±0.06	0.05
1.7	−3.06±0.05		
1.8	−2.85±0.06	0.14±0.08	0.025
2.0	−2.53±0.03	0.08±0.04	0.015
2.5	−1.77±0.03	−0.15±0.02	
3.0	−1.22±0.01	0.03±0.01	0.02±0.01
3.5	−0.833±0.003	0.02±0.01	0.02
4.0	−0.628±0.008	0.002±0.002	0.015
4.5	−0.490±0.004	−0.005±0.005	0.005
5.0	−0.393±0.002	−0.01±0.003	0.005
5.766	−0.295±0.001	−0.01±0.004	
6.0	−0.270±0.004	−0.011±0.005	−0.007
7.0	−0.200±0.004	−0.002±0.002	−0.001

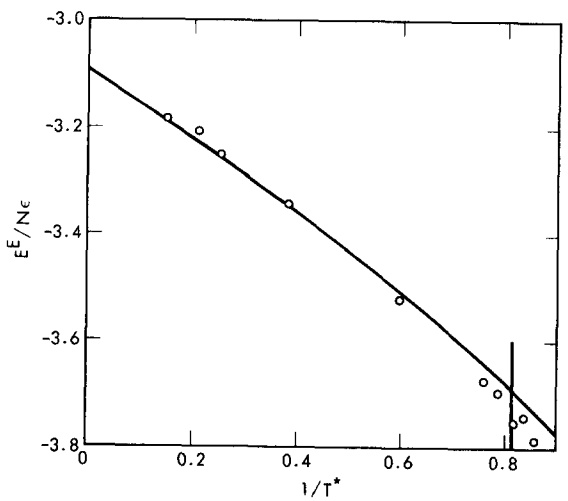

FIG. 12. Comparison of 108-particle molecular dynamics data (circles) with the four-term series approximation for the excess internal energy at $V/V_0=3.0$. The vertical mark indicates crossing of the liquid-gas coexistence curve.

The M distribution is very nearly gaussian about the average value $\langle M\rangle$ over the whole density range. This is demonstrated in Fig. (2) by direct comparison of an M distribution and a true gaussian. An examination of the ratios of the even fluctuation moments yields the same conclusion. Thus $\langle(M-\langle M\rangle)^4\rangle/3\langle(M-\langle M\rangle)^2\rangle^2$, $\langle(M-\langle M\rangle)^6\rangle/15\langle(M-\langle M\rangle)^2\rangle^3$, and $\langle(M-\langle M\rangle)^8\rangle/105\langle(M-\langle M\rangle)^2\rangle^4$ should all be unity if the distribution is gaussian. Table I shows that the ratios are indeed very close to unity. Since the gaussian function is an even function, all odd moments and hence all A_n's with odd $n\geq 3$ must be zero for such a distribution. Furthermore, all A_n's with even $n>2$ are also zero for a Gaussian distribution as the result of cancellation among the terms. Hence the nearly Gaussian M distribution implies that all A_n's with $n>2$ must be very small compared to A_2. This is turn means that good convergence of the series in Eq. (4) down to fairly low temperatures can be expected.

By direct calculation, the coefficient A_1 can be ob-

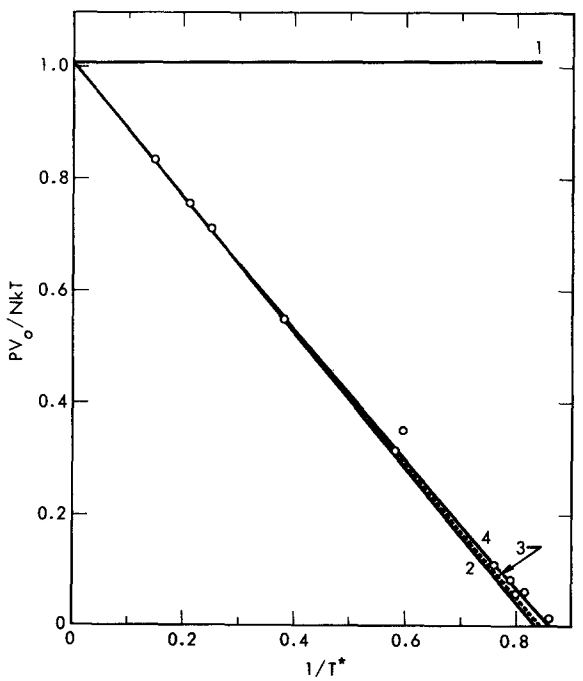

FIG. 11. Comparison of 108-particle molecular dynamics data (circles) with one-, two-, three-, and four-term series approximations for the pressure at $V/V_0=3.0$.

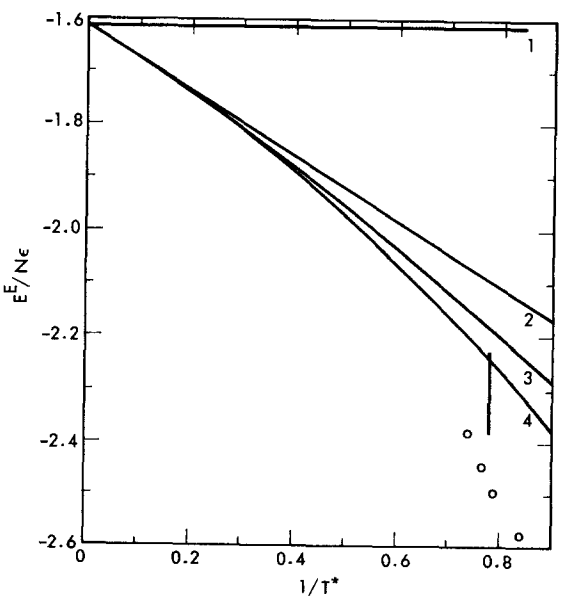

FIG. 13. Comparison of 108-particle molecular dynamics data (circles) and one-, two-, three-, and four-term series approximations for the excess internal energy at $V/V_0=5.0$. The vertical mark indicates crossing of the liquid-gas coexistence curve.

TABLE VII. Behavior of critical indices near the critical point for the square-well fluid with increasing numbers of expansion terms.

	Liquid				Gas			
	ρ_L/ρ_c [g]	α [h]	β [i]	γ [j]	ρ_G/ρ_C [g]	α [h]	β [i]	γ [j]
				$T/T_c=0.90$				
a	1.657	...	0.508	1.489	0.426	...	0.432	0.126
b	1.910	...	0.578	1.501	0.348	...	0.391	−0.037
c	1.652	...	0.522	1.442	0.415	...	0.447	−0.015
d	1.797	0.048	0.479	1.707	0.362	0.035	0.444	−0.222
e	1.791	0.058	0.463	1.696	0.352	0.065	0.445	−0.272
f	1.793	0.069	0.458	1.700	0.348	0.093	0.446	−0.285
				$T/T_c=0.93$				
a	1.548	...	0.510	1.412	0.509	...	0.449	0.336
b	1.742	...	0.563	1.428	0.435	...	0.416	0.225
c	1.542	...	0.518	1.385	0.503	...	0.463	0.237
d	1.669	0.031	0.505	1.630	0.457	0.025	0.463	0.086
e	1.668	0.039	0.489	1.639	0.450	0.045	0.466	0.041
f	1.670	0.048	0.486	1.650	0.446	0.065	0.467	0.026
				$T/T_c=0.96$				
a	1.412	...	0.510	1.317	0.620	...	0.467	0.548
b	1.544	...	0.547	1.333	0.556	...	0.441	0.482
c	1.406	...	0.513	1.307	0.618	...	0.478	0.490
d	1.500	0.016	0.532	1.448	0.583	0.015	0.473	0.419
e	1.503	0.022	0.521	1.447	0.577	0.025	0.475	0.393
f	1.506	0.028	0.520	1.489	0.575	0.036	0.475	0.384
				$T/T_c=0.99$				
a	1.203	...	0.505	1.157	0.805	...	0.489	0.811
b	1.259	...	0.523	1.176	0.765	...	0.474	0.784
c	1.200	...	0.507	1.165	0.805	...	0.492	0.786
d	1.238	0.004	0.528	1.169	0.785	0.004	0.482	0.784
e	1.242	0.006	0.527	1.179	0.782	0.006	0.481	0.778
f	1.243	0.007	0.529	1.181	0.781	0.008	0.480	0.777
				$T/T_c=0.998$				
c	1.089	...	0.504	1.060	0.912	...	0.499	0.916
d	1.103	0.001	0.508	1.046	0.901	0.001	0.489	0.912
e	1.105	0.001	0.507	1.047	0.900	0.001	0.488	0.909
f	1.105	0.002	0.511	1.046	0.899	0.002	0.484	0.908

[a] Classical van der Waals equation.
[b] van der Waals equation with correct hard sphere equation but constant a.
[c] First order perturbation theory.
[d] Second order perturbation theory.
[e] Third order perturbation theory.
[f] Fourth order perturbation theory.
[g] Coexistence densities relative to critical density.
[h] $C_V \propto (T-T_c)^{-\alpha}$.
[i] $(\rho_L-\rho_G) \propto (T-T_c)^{\beta}$.
[j] $-V(\partial p/\partial V)_T \propto (T-T_c)^{\gamma}$ along coexistence curve for $T<T_c$.

tained to 4–5 significant figures, A_2 to 2–3 significant figures and A_3 and A_4 to one significant figure. Higher terms cannot be obtained accurately by direct calculation. Generally speaking, the statistical method just described is better for the calculation of A_1 and A_2, and the graphical method described previously is better for the higher coefficients.

The statistical method fails for the calculation of higher A_n's because these quantities are extremely sensitive to small changes in the shape of the M distribution. Even a run as long as 15 million collisions for 108 particles is not sufficient to obtain high accuracy for A_3 and A_4. The problem is worse for larger systems because they undergo longer wavelength fluctuations which further increase the running time required to obtain true equilibrium averages. The number de-

pendence of A_1 and A_2 is too small to be detected by comparing 108 and 500 particle systems.

An alternative method for calculation of the higher A_n's involves repeating the calculation of M fluctuation moments at finite temperatures. Then the higher coefficients are related to the lower ones by the equation

$$A_{n+1}=\lim_{T\to\infty}(n+1)^{-1}\frac{\partial A_n(T^*)}{\partial(1/T^*)}. \qquad (10)$$

By numerically differentiating temperature dependent A_2 data, for example, A_3 may be obtained. Some values for A_3 and A_4 have been obtained in this manner.

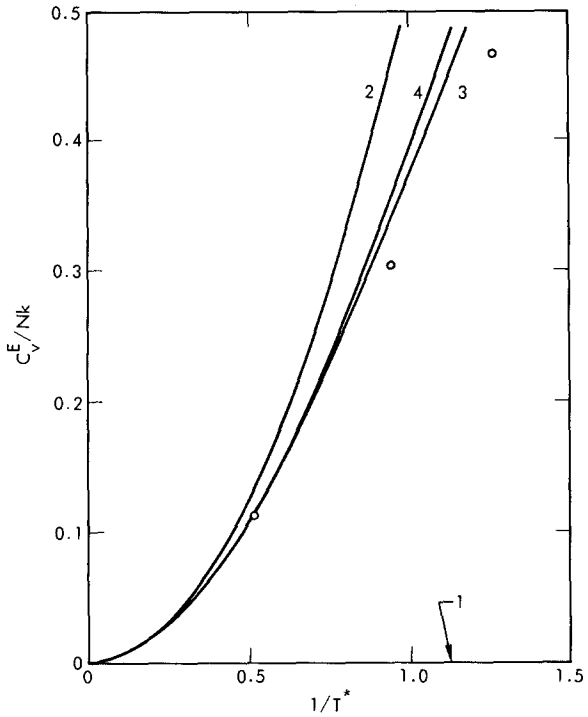

FIG. 14. Comparison of molecular dynamics excess heat capacity data (circles) with one-, two-, three-, and four-term series approximations at $V/V_0=1.6$.

In retrospect, the most accurate coefficients could be obtained by calculating A_1 and A_2 directly using the statistical method, and then using temperature dependent A_2 data to obtain A_3, A_4, and possibly higher coefficients by extrapolation.

IV. COEFFICIENTS

The A_n data are listed in Tables II–V and are shown in Figs. 3–6. The method of calculation is indicated, along with the number of particles and the uncertainty in each value of A_n.

The coefficient A_1 is given in somewhat different form than previously.[1] In terms of the quantity I defined previously, $A_1=-2\pi\sqrt{2}I/VN\epsilon$. The A_1 values calculated in the present paper are more accurate

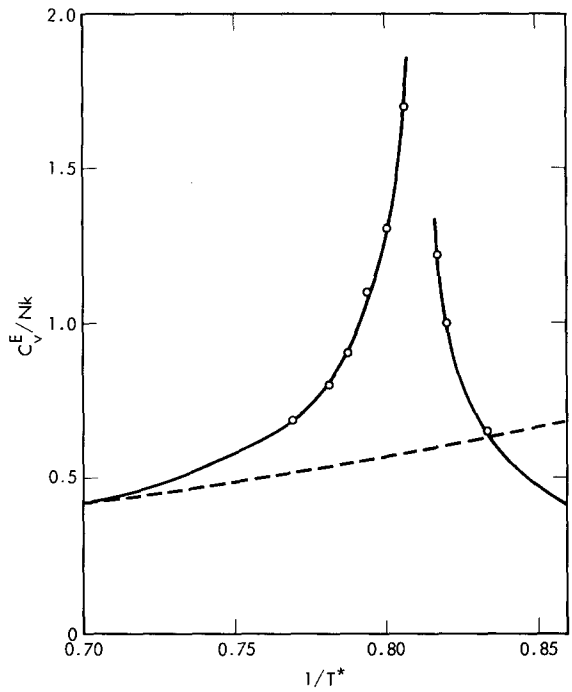

FIG. 15. Comparison of molecular dynamics excess heat capacity data (circles) obtained by numerical calculation of $(\partial E/\partial T)_V$ with the four-term series approximation (dashed curve) at $V/V_0=3.0$. The peak occurs near the coexistence curve.

than those calculated from I because integration over the numerical hard sphere pair distribution function is avoided. Previous Monte Carlo and theoretical calculations[4] of A_1 give results in quantitative agreement with this calculation. At close packing, each particle has 12 nearest neighbors and 6 second-nearest neighbors in its well. Hence $A_1=-18/2=-9$ in this limit. Also in the limit $V/V_0\to\infty$, A_1 must vanish. All higher A_n's vanish at both limits because density and hence energy fluctuations disappear at close packing as well as at zero density.

The functions A_1 and A_2 are both uniformly negative because $E^E<0$ and $-C_V{}^E<0$. Higher coefficients, however, change sign. The graph of A_2 in Fig. 4 shows some complex structure near $V/V_0=2.0$ and previous Monte Carlo and approximate theoretical calculations[4]

TABLE VIII. Critical constants estimated from molecular dynamics data for 32, 108, and 500 particles.

N	V_c/V_0	kT_c/ϵ	$p_cV_0/N\epsilon$	p_cV_c/NkT_c
32	4.65±0.30	1.308±0.005	0.101±0.001	0.359
108	4.40±0.20	1.290±0.005	0.096±0.001	0.326
500	4.25±0.25	1.260±0.005	0.085±0.002	0.287

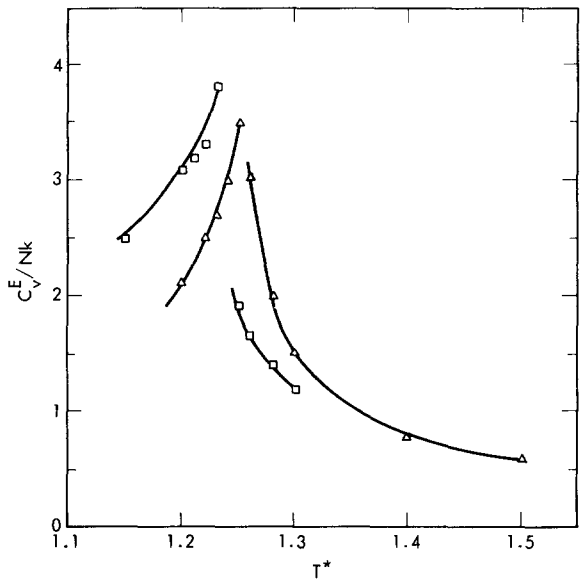

FIG. 16. Two heat capacity isochores at $V/V_0=4.0$ (triangles) and $V/V_0=5.0$ (squares) obtained from molecular dynamics data by numerical calculation of $(\partial E/\partial T)_V$ near the critical point.

are in substantial agreement with this result. However, a simple physical explanation of the structure is not apparent. The value of A_2 at $V/V_0=1.5$ near the freezing point is only 3% of the corresponding value of A_1, and A_3 is only 0.5% of A_1. Thereafter, convergence appears to slow down since A_4 is of the same magnitude as A_3. Nevertheless, this confirms the first-order augmented van der Waals theory as an accurate approximation for dense fluids.

It is apparent in Figs. 3–6 that the contributions to the A_n's from the first four virial coefficients (second through fifth) of the square-well potential[5] do an increasingly poor job of fitting the A_n data in the volume range considered. This happens because the higher A_n's involve larger numbers of correlated particles and hence have nonasymptotic structure at larger characteristic values of V/V_0 before they drop asymptotically to zero. In addition, exact calculations with the one-dimensional square-well fluid show that at high density the higher coefficients have more complex structure, such as maxima and minima, than do the lower coefficients. Unfortunately, the larger uncertainties in the calculated three-dimensional molecular dynamics results obscure any small structure in A_3 or A_4. In Figs. 3–6 smooth curves have been drawn (as shown) through the data points, and these curves have been fit by a least squares method to polynomial functions in powers of V_0/V. The coefficients used in the polynomials are listed in Appendix II.

The coefficients p_n in the expansion of the pressure have also been calculated. The calculations have been done by reduction of the molecular dynamics equation of state data in the same way as with the excess internal energy. No direct hard sphere fluctuation calculations have been carried out for the p_n's, although such calculations are possible. Consistency between the A_n's and p_n's through the relationship Eq. (8) is checked by comparison of the volume derivative of the polynomial fit to each A_n with the direct (graphical) evaluation of the corresponding p_n. These comparisons are shown in Figs. 7–9, and the consistency is satisfactory. The molecular dynamics data give out at p_3, and hence p_4 cannot be obtained by the graphical method. A graph of p_4 computed from the volume derivative of A_4 is given in Fig. 10. The p_n data are listed in Table VI. Note again the decrease of successive p_n terms in the dense fluid by an order of magnitude up to p_4, which is the same magnitude as p_3.

A simple way of checking how well the finite reciprocal temperature series represents the data and hence to what temperature the expansion converges is to compute the thermodynamic functions by the use of Eqs. (6)–(8) and see how well the results compare with the molecular dynamics data. Examples are shown in Figs. 11–14. In general, the pressure for $T^*\geq 1.0$ is well represented by three coefficients (Fig. 11). For the internal energy the data are well represented for $T^*\geq 1.0$ by four coefficients for volumes $V/V_0\leq$

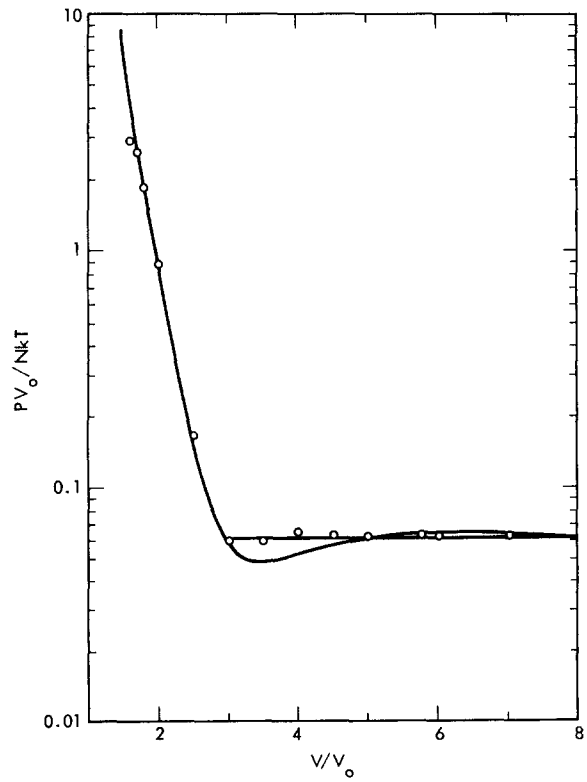

FIG. 17. Comparison of a pressure isotherm at $T^*=1.25$ obtained from interpolated molecular dynamics data (circles) with the four-term series approximation (smooth curve). The horizontal line marks the estimated liquid-gas tie line.

TABLE IX. Comparison of critical constants calculated from 1, 2, 3, and 4 term virial and $1/T^*$ expansions with molecular dynamics (MD) estimate.

Number of terms	V_c/V_0		kT_c/ϵ		$p_cV_0/N\epsilon$		p_cV_0/NkT_c	
	Virial	$1/T$	Virial	$1/T$	Virial	$1/T$	Virial	$1/T$
1	...	4.56	...	1.404	...	0.136	...	0.441
2	4.95	4.72	1.33	1.354	0.090	0.111	0.333	0.387
3	8.33	4.67	1.16	1.330	0.051	0.105	0.366	0.359
4	10.00	4.67	1.13	1.318	0.047	0.102	0.416	0.351
				108 particles				
MD	4.40±0.20		1.290±0.005		0.096±0.001		0.326	

3.0 (Fig. 12). For volumes $V/V_0 \geq 3.0$ the finite sum obviously fails to reproduce the data (Fig. 13), and more coefficients are needed. The convergence in the range $V/V_0 \approx 4$–5 and $T^* \approx 1$ is poor because this is the critical region of the fluid. Singular behavior in C_V^E and its derivatives is expected in this region, and expansions of these functions will not converge because of the large fluctuations present.

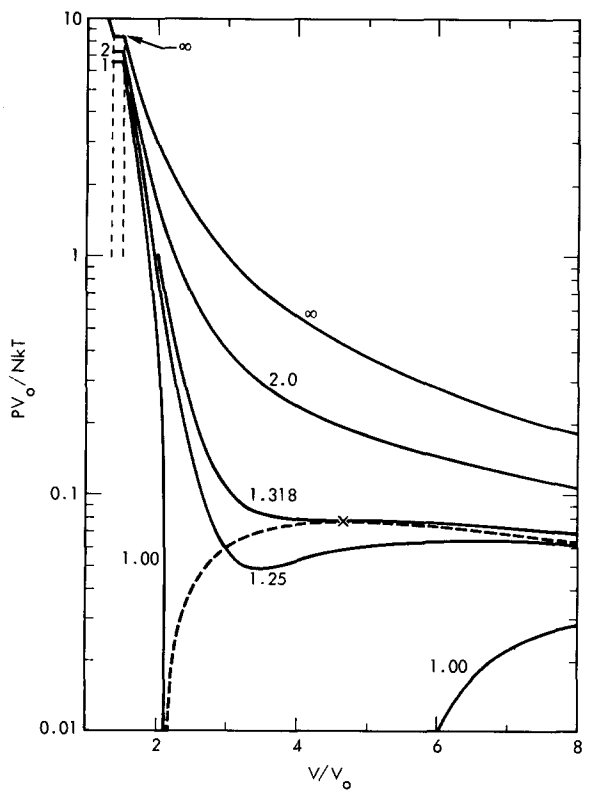

FIG. 18. Pressure isotherms calculated from the four-term series approximation for the subcritical temperatures $T^*=1.00$, and 1.25, the critical temperature $T^*=1.318$, and the supercritical temperatures $T^*=2.00$ and ∞. The liquid-solid coexistence region is indicated as well as the tie lines for $T^*=\infty$, 2.00, and 1.00. The liquid-gas coexistence curve is shown as a dashed curve and the critical point is marked by a cross.

Excess heat capacity data at $V/V_0=1.6$ are shown in Fig. 14 and are fitted fairly well by a three-term series. The data points are calculated from temperature dependent values of A_2 (See Appendix I). The failure of the three-term series for C_V^E is clearly shown in Fig. 15, where a sharp peak appears upon crossing the coexistence curve. A pair of heat capacity isochores bracketing the critical point is given in Fig. 16. Each curve shows singular behavior near $T^*=1.25$, again as the result of crossing the coexistence curve. The C_V^E data points in Figs. 15 and 16 were computed by numerical differentiation of the excess internal energy with respect to T^*. For finite systems of particles the value of the heat capacity cannot actually become infinite, but in fact it becomes sufficiently large that a sharp peak occurs with a high maximum value. The height of this maximum will increase indefinitely with increasing system size.

The above comparisons have all been made along isochores. A comparison of pressures obtained from the

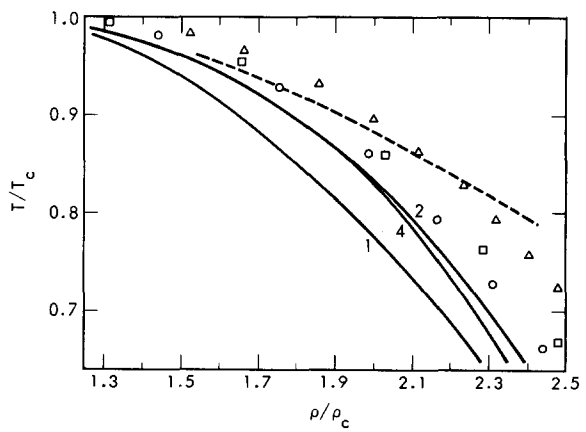

FIG. 19. Comparison of the liquid branch of the coexistence curve as predicted by the first (1), second (2), and fourth (4) order perturbation theory with experiment (○-argon, □-krypton, and △-xenon). The dashed curve results from the van der Waals theory with a constant "a" value and a correct hard sphere equation of state.

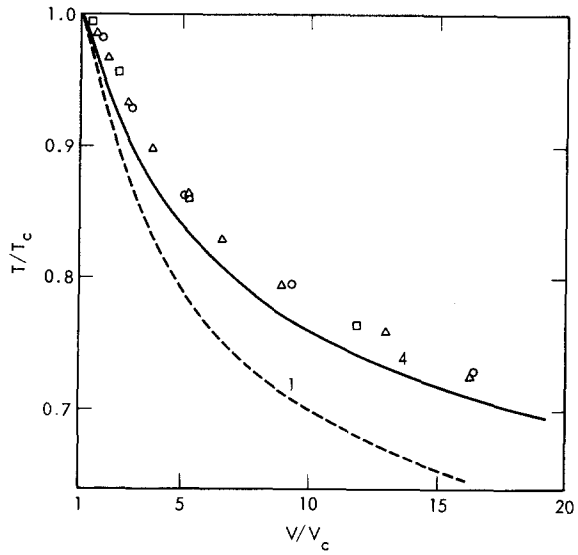

FIG. 20. Comparison of the gas branch of the coexistence curve as predicted by the first (1) and fourth (4) order perturbation theory with experiment (O-argon, □-krypton, and △-xenon).

four-term series and from interpolated molecular dynamics data along the $T^*=1.25$ isotherm is shown in Fig. 17. The comparison is very accurate except that in the two-phase region the four-term series has deeper van der Waals loops than the nearly flat molecular dynamics data.

V. CRITICAL REGION

In Fig. 18 four-term series pressure isotherms are shown. The top-most isotherm is the hard sphere isotherm, and lower isotherms correspond to finite temperatures as indicated. The hard sphere isotherm shows a phase transition at $V/V_0=1.5$, where the fluid coexists with the solid. Calculation of the coefficients in the free energy expansion can be made for the solid phase as well as the fluid phase, and this is now being carried out. The details of the augmented van der Waals theory and its corrections for the square-well solid will be published later, but the fluid-solid coexistence curve has been calculated to second order in perturbation theory by matching the Gibbs free energies of the fluid and solid. The coexistence curve has been sketched in Fig. 18.

In Fig. 18 the critical isotherm appears with its characteristic inflection point, and below this isotherm van der Waals loops occur. The coexisting liquid and vapor densities and pressures are then determined by the Maxwell equal area rule. The liquid–gas coexistence curve is sketched in Fig. 18 and numerically given in Table VII. In Figs. 19 and 20 these coexistence curves are shown in greater detail and compared to experiments, with the conclusion that the fourth order perturbation theory leads to a greatly improved shape

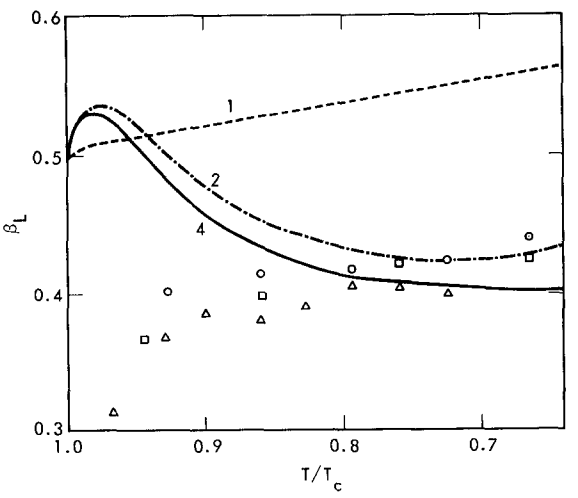

FIG. 21. Comparison of the critical exponent β_L on the liquid side of the coexistence curve at various temperatures relative to the critical temperature for the first (1), second (2), and fourth (4) order perturbation theory with experiment (O-argon, □-krypton, △-xenon).

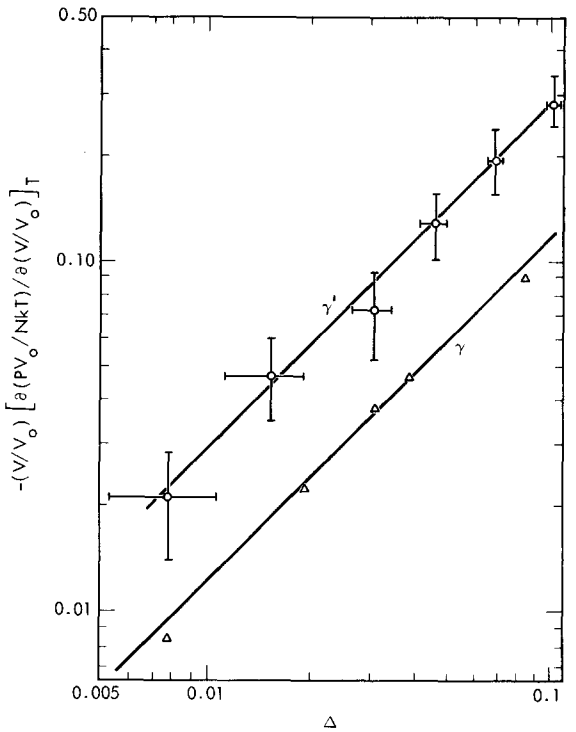

FIG. 22. Determination of the indices γ and γ' for 108 particles by plotting

$$-\left(\frac{V}{V_0}\right)\left[\frac{\partial(pV_0/NkT)}{\partial(V/V_0)}\right]_T \quad \text{vs} \quad \Delta=(T-T_c)/T_c.$$

Error bars are indicated on γ' and are similar to those on γ. ($\gamma=\gamma'=1.0\pm0.1$).

TABLE X. Comparison of critical point indices estimated from molecular dynamics data with indices obtained from the van der Waals model, the lattice gas Ising model, and experiment (see Ref. 6).

	α	α'	β	γ	γ'	δ
van der Waals	0	0	0.50	1.0	1.0	3.0
Lattice gas	0.07±0.1	0.1±0.1	0.313±0.004	1.250±0.001	1.31±0.05	5.2±0.15
Experiment	0.2±0.2	0.12±0.12	0.346±0.01	1.37±0.2	1.0±0.3	4.4±0.4
Molecular dynamics	0.20±0.1	0.12±0.1	0.50±0.05	1.0±0.1	1.0±0.1	3.0±0.3

compared to the first order theory. It is also apparent that the major improvement comes from adding the second order term; the third and fourth order terms generally bring about small quantitative contributions.

The critical constants themselves have been estimated from molecular dynamics data for 32, 108, and 500 particles. From the results given in Table VIII it can be seen that the values depend sensitively on the number of particles. The effect of the larger system is to flatten the top of the coexistence curve. These results can be compared to the curves obtained by using successively higher order terms in the perturbation series as shown in Table IX. The theoretical critical volume, temperature, pressure, and compressibility factor differ from the 108 particle molecular dynamics results by 5, 2, 9, and 12%, respectively, in the four-term approximation. The 108 particle results have been used throughout since the A_n coefficients were derived primarily from 108 particle data. The inverse temperature series is obviously much more effective in predicting the critical points than is the virial series, whose predictions are also given in Table IX.

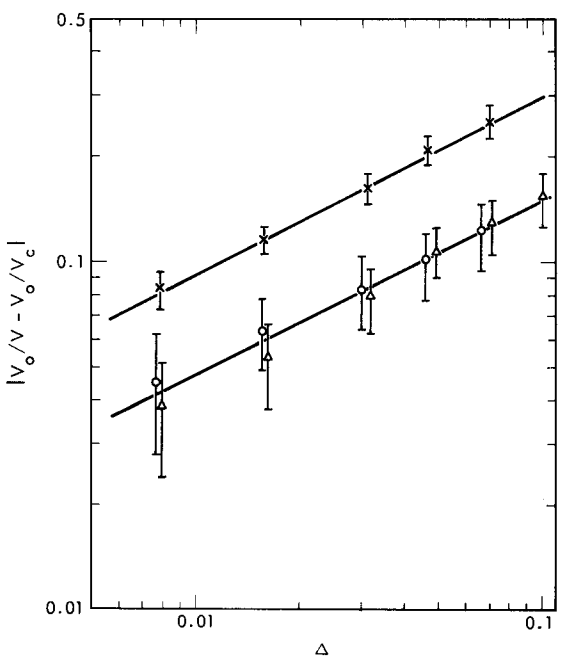

FIG. 23. Determination of the exponent β for 108 particles in the liquid phase (triangles) and gas phase (circles) by plotting $|V_0/V - V_0/V_c|$ vs $\Delta=(T-T_c)/T_c$. Error bars are indicated. The line through the crosses plots $V_0/V_L - V_0/V_G$ vs Δ, leading to the same value of β. ($\beta=0.5\pm0.05$).

The behavior of the critical indices is predicted incorrectly by the perturbation theory, as it is for any theory which is analytic. The indices which determine the behavior of thermodynamic functions near the critical point are defined as follows:[6]

$$\Delta=(T-T_c)/T_c$$

α: $C_V\sim\Delta^{-\alpha}$ $\quad\rho=\rho_c$, $\Delta>0$

α': $C_V\sim(-\Delta)^{-\alpha'}$ $\quad\rho=\rho_c$, $\Delta<0$

β: $(\rho_L-\rho_G)\sim(-\Delta)^{\beta}$ $\quad\Delta<0$, coexistence curve

γ: $\kappa_T\sim\Delta^{-\gamma}$ $\quad\rho=\rho_c$, $\Delta>0$

γ': $\kappa_T\sim(-\Delta)^{-\gamma'}$ $\quad\Delta<0$, coexistence curve

δ: $|p-p_c|\sim|\rho-\rho_c|^{\delta}$ $\quad T=T_c$.

Here ρ_L and ρ_G are the coexisting liquid and gas densities, and κ_T is the isothermal compressibility. It was thought worthwhile to evaluate the indices away from the critical point for the four-term series to see whether they approach realistic values. As Table VII shows, the indices at $T/T_c=0.9$ generally have moved in the correct direction away from the van der Waals values, and as Fig. 21 shows, at values of T/T_c even farther away from the critical point, some indices compare quite well with experiment.[7,8]

The indices can also be obtained directly from molecular dynamics data by a graphical analysis similar to what is done with experimental data. Such an analysis is shown in Figs. 22–24 and summarized in Table X. Within the rather large experimental uncertainty it is clear that the molecular dynamics critical indices also follow the predictions of the van der Waals theory except for the heat capacity indices α and α'. The accurate values of α and α' are not surprising in view of the realistic heat capacity peaks observed earlier in Figs. 15 and 16. The van der Waals value of the other coefficients must be ascribed to the smallness of the

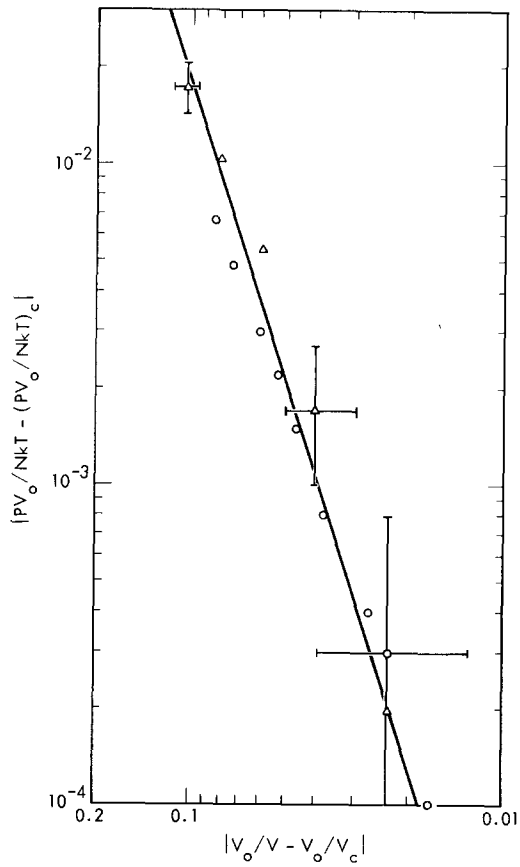

FIG. 24. Determination of the exponent δ for 108 particles in the liquid phase (triangles) and gas phase (circles) by plotting $|pV_0/NkT-(pV_0/NkT)_c|$ vs $|V_0/V-V_0/V_c|$ along the critical isotherm. Typical error bars, which increase as V approaches V_c, are indicated. ($\delta=3.0\pm0.2$).

molecular dynamic systems investigated. Evidently, the top of the coexistence curve flattens out only very slowly with increasing system size, depending sensitively on long-range spatial correlations. The heat capacity, however, appears to be less sensitive to these correlations.

VI. CONCLUSION

The corrections to the augmented van der Waals pressure equation of state outside the critical region and at $V<V_c$ are small because they involve volume and temperature derivatives of the slowly varying heat capacity term $T^2C_V^E$. For the Helmholtz free energy, the second order term involving the heat capacity must be taken into account, but higher terms are again small because of the temperature insensitivity of $T^2C_V^E$. Thus a major improvement in the thermodynamic description should come about if the second order term, namely A_2/T^{*2}, were kept in the free energy expansion. For the square-well fluid, the reduced excess heat capacity can be well approximated by the first term in Eq. (7), namely $-2A_2/T^{*2}$. As long as the higher terms, however many, are density independent, the pressure equation of state remains unaffected ($p_n=0$) and no inconsistency arises about the number of terms kept. Furthermore, for the square-well fluid, $-2A_2\cong0.5$, so that $C_V^E/Nk\cong1.4$ at $T^*=0.6$ near the melting point. The high temperature approximation for the heat capacity, however, clearly has the wrong temperature dependence at low temperatures. A practical procedure for correcting this might be to assume that the higher perturbation terms in the heat capacity sum up to a constant heat capacity at low temperatures. In other words, the heat capacity should be $C_V^E/Nk=-2A_2/T^{*2}$ at high temperatures and should smoothly connect to the value 1.5 known to be valid at low temperatures.

ACKNOWLEDGMENTS

We wish to thank Mary Ann Mansigh for her skilled programming effort and great persistence over the years which it took to finish this project. We also wish to thank K. Miller, R. Linford, and R. Powell for help in evaluating the critical indices.

APPENDIX A

The raw data obtained from molecular dynamics calculations is tabulated below. The number of particles (N), reduced temperature (T^*), reduced excess internal energy ($-E^E/N\epsilon$), and reduced pressure (pV_0/NkT) are given for each run. A table of excess heat capacity data appears at the end of the Appendix. The uncertainty in T^* and $-E^E/N\epsilon$ is about 0.5%, and in pV_0/NkT and C_V^E/Nk, about 1%.

$V/V_0=1.6$

N	T^*	$-E^E/N\epsilon$	pV_0/NkT
108	11.2	6.173	5.96
108	6.76	6.196	5.88
108	3.50	6.299	5.54
108	2.41	6.305	5.22
108	1.94	6.347	4.82
108	1.90	6.349	4.79
108	1.41	6.425	4.30
108	1.06	6.535	3.66
108	0.945	6.584	3.33
108	0.792	6.661	2.86
108	0.781	6.671	2.78
108	0.707	6.728	2.45
108	0.670	6.755	2.19
108	0.648	6.772	2.13
108	0.588	6.833	1.76
108	0.411	7.132	−0.21
500	1.41	6.424	4.28
500	0.584	6.825	1.79

$V/V_0=1.7$

N	T^*	$-E^E/N\epsilon$	pV_0/NkT
108	10.98	5.803	4.77
108	6.73	5.873	4.59
108	3.31	5.958	4.12
108	1.73	6.095	3.31
108	1.44	6.168	3.00
108	1.03	6.295	2.25
108	0.725	6.462	1.24
108	0.676	6.514	0.99
108	0.606	6.575	0.61
108	0.577	6.616	0.41
108	0.520	6.680	0.01
108	0.503	6.704	−0.11

$V/V_0=1.8$

N	T^*	$-E^E/N\epsilon$	pV_0/NkT
108	6.36	5.563	3.70
108	3.11	5.665	3.17
108	2.05	5.750	2.77
108	1.57	5.855	2.28
108	1.30	5.949	1.88
108	1.10	5.986	1.53
108	0.786	6.179	0.63
108	0.663	6.290	0.07
108	0.629	6.312	−0.11
108	0.60	6.328	−0.16
108	0.59	6.389	−0.32

$V/V_0=2.0$

N	T^*	$-E^E/N\epsilon$	pV_0/NkT
32	5.46	5.02	2.52
32	3.22	5.10	2.18
32	2.48	5.14	1.94
32	0.80	5.67	−0.26
32	0.62	6.16	−1.68
32	0.427	6.18	−3.14
108	6.38	5.018	2.52
108	5.99	5.036	2.40
108	2.73	5.121	2.00
108	2.63	5.150	1.95
108	2.13	5.232	1.72
108	1.74	5.277	1.44
108	1.34	5.376	1.01
108	1.261	5.403	0.91
108	1.012	5.480	0.39
108	0.900	5.592	0.09
108	0.895	5.596	0.06
108	0.606	5.914	−1.25
108	0.570	6.026	−1.44
108	0.461	6.194	−2.28
500	6.11	5.027	2.51
500	1.77	5.274	1.47
500	0.87	5.614	0.01

$V/V_0=2.5$

N	T^*	$-E^E/N\epsilon$	pV_0/NkT
32	8.79	3.90	1.37
32	4.75	3.95	1.22
32	2.53	4.06	0.87
32	1.82	4.14	0.62
32	0.990	4.43	−0.18
32	0.693	4.75	−0.96
32	0.461	5.17	−2.19
108	2.09	4.08	0.71
108	1.26	4.36	0.16
108	1.15	4.40	0.04
108	0.80	4.71	−0.42

$V/V_0=3.0$

N	T^*	$-E^E/N\epsilon$	pV_0/NkT
32	4.26	3.22	0.73
32	2.05	3.36	0.44
32	1.41	3.52	0.18
32	0.98	3.79	−0.14
32	0.75	4.07	−0.45
32	0.55	4.53	−0.67
32	0.417	4.79	−1.17
32	0.393	5.06	−7.15
32	0.387	5.43	−7.73
32	0.265	5.94	−8.11
108	6.91	3.18	0.84
108	4.83	3.21	0.76
108	4.03	3.25	0.71
108	2.62	3.34	0.55
108	1.68	3.52	0.30
108	1.32	3.672	0.11
108	1.27	3.695	0.08
108	1.23	3.750	0.06
108	1.16	3.785	0.01
108	0.895	4.025	−0.19
108	0.686	4.541	−0.41
108	0.557	4.845	−0.63
108	0.280	5.922	−8.12
500	4.91	3.234	0.76
500	1.73	3.518	0.31

$V/V_0=3.5$

N	T^*	$-E^E/N\epsilon$	pV_0/NkT
108	1.293	3.234	0.084
108	1.246	3.269	0.057
108	1.204	3.308	0.036
108	1.165	3.346	0.015
500	1.276	3.311	0.077
500	1.240	3.359	0.062
500	1.205	3.399	0.047

$V/V_0=4.0$

N	T^*	$-E^E/N\epsilon$	pV_0/NkT
32	7.63	2.26	0.47
32	5.39	2.29	0.45
32	4.64	2.37	0.43
32	3.12	2.38	0.36
32	2.44	2.46	0.30
32	1.99	2.53	0.25
32	1.20	2.88	0.03
32	0.89	3.18	−0.10
32	0.80	3.43	−0.17
32	0.61	3.84	−0.34
32	0.58	4.09	−0.36
108	1.302	2.918	0.079
108	1.245	2.984	0.058
108	1.240	2.981	0.055
108	1.190	3.049	0.040
108	1.144	3.103	0.025
108	1.081	3.326	0.005
500	3.015	2.443	0.348
500	1.266	3.008	0.070
500	1.240	3.067	0.061
500	1.200	3.140	0.048

$V/V_0=4.5$

N	T^*	$-E^E/N\epsilon$	pV_0/NkT
32	1.370	2.500	0.089
32	1.300	2.531	0.076
32	1.247	2.573	0.057
32	1.189	2.679	0.039
108	1.304	2.651	0.078
108	1.268	2.696	0.068
108	1.223	2.735	0.053
108	1.201	2.790	0.049
108	1.178	2.843	0.040
500	1.730	2.423	0.170
500	1.311	2.703	0.081
500	1.306	2.712	0.079
500	1.265	2.782	0.069
500	1.249	2.824	0.068
500	1.237	2.884	0.062
500	1.196	2.955	0.050

$V/V_0=5.0$

N	T^*	$-E^E/NkT$	pV_0/NkT
32	7.38	1.750	0.327
32	5.07	1.800	0.301
32	4.27	1.811	0.289
32	2.80	1.899	0.237
32	2.13	1.990	0.207
32	2.10	2.000	0.190
32	1.70	2.091	0.149
32	1.317	2.297	0.079
32	1.290	2.317	0.073
32	1.264	2.334	0.068
32	1.242	2.380	0.061
32	1.211	2.388	0.054
32	1.023	2.616	−0.005
32	0.813	3.066	−0.087
32	0.701	3.279	−0.132
32	0.570	3.772	−0.198
32	0.438	4.020	−0.307
108	1.361	2.382	0.087
108	1.309	2.446	0.076
108	1.273	2.493	0.069
108	1.200	2.578	0.053
108	1.155	2.676	0.041
108	1.128	2.768	0.029

N	T^*	$-E^E/N\epsilon$	pV_0/NkT
500	1.335	2.475	0.083
500	1.277	2.560	0.069
500	1.217	2.689	0.055
500	1.208	2.722	0.053

$V/V_0=5.766$

N	T^*	$-E^E/N\epsilon$	pV_0/NkT
108	1.332	2.162	0.078
108	1.272	2.228	0.068
108	1.221	2.283	0.059

$V/V_0=6.0$

N	T^*	$-E^E/N\epsilon$	pV_0/NkT
108	11.6	1.435	0.258
108	1.310	2.118	0.075
108	1.240	2.200	0.060
108	1.202	2.290	0.053
108	1.164	2.358	0.045

$V/V_0=7.0$

N	T^*	$-E^E/N\epsilon$	pV_0/NkT
108	1.330	1.850	0.073
108	1.280	1.905	0.067
108	1.196	2.062	0.053
108	1.152	2.154	0.044

$V/V_0=1.6$

N	T^*	$\langle(M-\langle M\rangle)^2\rangle/N$	C_V^E/Nk
108	∞	0.512	0
108	1.941	0.423	0.112
108	1.060	0.340	0.302
108	0.792	0.291	0.464

$V/V_0=2.0$				$V/V_0=3.0$			
N	T^*	$\langle(M-\langle M\rangle)^2\rangle/N$	C_V^E/Nk	N	T^*	$\langle(M-\langle M\rangle)^2\rangle/N$	C_V^E/Nk
108	∞	0.612	0	108	∞	0.612	0
108	6.378	0.601	0.015	108	6.914	0.646	0.014
108	2.630	0.588	0.085	108	4.029	0.694	0.043
108	1.342	0.495	0.275	108	2.625	0.710	0.103
108	0.900	0.383	0.473	108	1.199	0.779	0.542

APPENDIX B

The first four virial coefficients of the square-well potential are known as functions of T^* (Ref. 5) and each of these contains a contribution to each coefficient A_n in the $1/T^*$ expansion. The virial coefficient contribution to the first four A_n's are given below:

B_2	B_3	B_4	B_5
$A_1=-7.03/(V/V_0)$	$-7.27/(V/V_0)^2$	$-1.25/(V/V_0)^3$	$+6.08/(V/V_0)^4$
$A_2=-3.52/(V/V_0)$	$+11.15/(V/V_0)^2$	$-2.17/(V/V_0)^3$	$-41.6/(V/V_0)^4$
$A_3=-1.17/(V/V_0)$	$+7.15/(V/V_0)^2$	$-31.3/(V/V_0)^3$	$+170/(V/V_0)^4$
$A_4=-0.29/(V/V_0)$	$-1.32/(V/V_0)^2$	$+32.9/(V/V_0)^3$	$-164/(V/V_0)^4$

Polynomial fits have been obtained for the A_n of the form

$$A_n=\sum_{m=1}^{M}\frac{A_{nm}}{(V/V_0)^m}.$$

The A_{nm} are given as follows:

$A_{11}=-7.0346$
$A_{12}=-7.2736$
$A_{13}=-1.2520$
$A_{14}=6.0825$
$A_{15}=6.8$
$A_{16}=1.7$

$A_{20}=-0.12495816\times10^{-3}$
$A_{21}=-0.33015580\times10^{1}$
$A_{22}=-0.98155782\times10^{0}$
$A_{23}=+0.22022115\times10^{3}$
$A_{24}=-0.19121478\times10^{4}$
$A_{25}=+0.86413158\times10^{4}$
$A_{26}=-0.22911464\times10^{5}$
$A_{27}=+0.35388809\times10^{5}$
$A_{28}=-0.29353643\times10^{5}$
$A_{29}=+0.10090478\times10^{5}$

$A_{30}=-0.51235572\times10^{-4}$
$A_{31}=-0.11868777\times10^{1}$
$A_{32}=+0.72447507\times10^{1}$
$A_{33}=-0.17432407\times10^{2}$
$A_{34}=+0.19666211\times10^{2}$
$A_{35}=-0.85145188\times10^{1}$

$A_{40}=+0.25364174\times10^{-2}$
$A_{41}=-0.51739049\times10^{0}$
$A_{42}=+0.25259812\times10^{1}$
$A_{43}=-0.41246808\times10^{1}$
$A_{44}=+0.23434564\times10^{1}$

The polynomial fit to A_1 is based on the virial expansion, but A_2, A_3, and A_4 have been fit directly by a computer program. It is necessary to keep the significant figures shown because of extensive cancellations among the terms. The A_{n0} terms are artifacts of the approximate fitting routine and they have no effect on the pressure. Values of p_n may be calculated from A_n simply by

$$p_n=\sum_{m=1}^{M}\frac{mA_{nm}}{(V/V_0)^{m+1}}.$$

* Work performed under the auspices of the U.S. Atomic Energy Commission.

† Present Address: Civil Engineering Department, Stanford University, Stanford, Calif. 94305.

[1] B. J. Alder and C. E. Hecht, J. Chem. Phys. **50,** 2032 (1969).
[2] The classical van der Waals equation of state is $pV/NkT=[V/(V-b)]-(a/NkTV)$.
[3] R. W. Zwanzig, J. Chem. Phys. **22,** 1420 (1954).
[4] J. A. Barker and D. Henderson, *Proceedings of the Fourth Symposium on Thermophysical Properties,* edited by J. R. Moszynski (ASME, New York, 1968) p. 30; J. A. Barker and D. Henderson, J. Chem. Phys. **47,** 2856 (1967).
[5] J. A. Barker and D. Henderson, Can. J. Phys. **45,** 3959 (1967).
[6] L. P. Kadanoff *et al.*, Rev. Mod. Phys. **39,** 395 (1967).
[7] G. A. Cook, *Argon, Helium, and the Rare Gases* (Interscience, New York, 1961).
[8] M. J. Terry, J. T. Lynch, M. Bunclark, K. R. Mansell, and L. A. K. Stavely, J. Chem. Thermodyn. **1,** 413 (1969).